Energy 112 (2016) 481–493

Contents lists available at ScienceDirect

Energy

journal homepage: www.elsevier.com/locate/energy

Effects of adsorbent mass and number of adsorber beds on the performance of a waste heat-driven adsorption cooling system for vehicle air conditioning applications

Amir Sharafian, Seyyed Mahdi Nemati Mehr, Poovanna Cheppudira Thimmaiah, Wendell Huttema, Majid Bahrami*

Laboratory for Alternative Energy Conversion (LAEC), School of Mechatronic Systems Engineering, Simon Fraser University, BC, V3T 0A3, Canada

ARTICLE INFO

Article history:
Received 8 August 2015
Received in revised form
18 June 2016
Accepted 20 June 2016
Available online 5 August 2016

Keywords:
Adsorbent mass
FAM-Z02
Adsorber bed
Adsorption cooling system
Vehicle air conditioning

ABSTRACT

Waste heat-driven adsorption cooling systems (ACS) are potential replacements for vapor compression refrigeration cycles in vehicle air conditioning applications. However, the bulkiness and heavy weight of ACS are major challenges facing commercialization of these environmentally friendly systems. This study examines the effects of adsorbent mass and the number of adsorber beds on the performance of a FAM-Z02/water ACS under different operating conditions. The experimental results show that reducing the mass of FAM-Z02 from 1.9 to 0.5 kg in a one-adsorber bed ACS increases the SCP by 82% from 65.8 to 119.4 W/kg at cycle time of 20 min. However, the COP reduces by 37% because of the increase in the adsorber bed to adsorbent mass ratio. The results also show that the thermal mass of the evaporator limits the performance of the ACS, especially under short cycle times (8–20 min). A second adsorber bed is added to the one-adsorbed bed ACS test bed to generate continuous cooling in the evaporator. Comparing the performance of one- and two-adsorber bed ACS packed with 0.5 kg of FAM-Z02 particles and cycle time of 20 min shows that the SCP and COP of the two-adsorber bed ACS increase by 28% and 47%, respectively.

1. Introduction

Air conditioning and refrigeration (A/C-R) systems are responsible for using about 30% of the total worldwide energy produced [1]. In the automotive sector, A/C systems of light-duty vehicles consume about 40 billion liters of fuel per year in the U.S. alone [2]. A compressor of a vapor compression refrigeration cycle (VCRC) installed in a typical medium size sedan consumes up to 5–6 kW of the power generated by an internal combustion engine (ICE) to produce the required cooling. This power is sufficient for a 1200-kg sedan to cruise at 56 km/h [2]. Furthermore, about 70% of the total fuel energy released in an ICE is dissipated as a waste heat through the engine coolant and the exhaust gas [3]. Waste heat-driven adsorption cooling systems (ACS) are potential replacements for VCRCs that can significantly reduce fuel consumption and the environmental impacts of A/C systems where low-grade thermal energy is available.

A waste heat-driven ACS uses an adsorbate, such as water or methanol, which is adsorbed and desorbed from the surface of a porous adsorbent, such as zeolite, silica gel, or activated carbon. Most of these materials are non-toxic, non-corrosive, and inexpensive [4], making ACS a safe and environmentally friendly technology. An ACS operates more quietly than a VCRC and is easier to maintain because its only moving parts are valves [5]. However, current ACS have not been commercialized for light-duty vehicles due to their bulkiness and heavy weight. The main challenges facing this technology are low specific cooling power (SCP = cooling energy/(adsorbent mass × cycle time)) and coefficient of performance (COP = cooling energy/input energy) that originate from the low thermal conductivity of adsorbent particles (~0.1–0.4 W/m.K) [6–9] and the low mass diffusivity of adsorbent-adsorbate pairs (~10^{-8}–10^{-14} m^2/s) [7,10].

To overcome these obstacles, different composite adsorbent materials with high thermal conductivity and high adsorbate

* Corresponding author. School of Mechatronic Systems Engineering, Simon Fraser University, # 4300, 250-13450 102nd Avenue, Surrey, BC, V3T0A3, Canada.
E-mail addresses: asharafi@sfu.ca (A. Sharafian), snematim@sfu.ca (S.M. Nemati Mehr), pthimmai@sfu.ca (P.C. Thimmaiah), wah@sfu.ca (W. Huttema), mbahrami@sfu.ca (M. Bahrami).

http://dx.doi.org/10.1016/j.energy.2016.06.099
0360-5442/

uptake capacity have been developed such as the ones reported in Refs. [11,12]. Besides using a proper adsorbent material, the designs of the adsorber beds, condenser, and evaporator (the main components of an ACS) can significantly affect the SCP and COP of the system. Sharafian and Bahrami [13] conducted a comprehensive literature review on the effects of nine different adsorber bed designs on the performance of an ACS designed for vehicle A/C applications. They identified the SCP, adsorber bed to adsorbent mass ratio (AAMR), and COP as the most influential parameters for evaluating the performance of an ACS. The COP was found to have a lower importance than the SCP and AAMR because the supplied waste heat for regeneration of the adsorber beds was abundant in a vehicle [13]. However, an ACS with a higher COP was preferred. The AAMR represents the dead to active mass ratio and should be minimized for vehicle A/C applications. Comparing more than 66 experiments with different adsorber bed designs reported in the literature showed that finned tube adsorber beds provided the best performance in comparison with other types of adsorber bed designs [13]. Table 1 provides further details on the performance of waste heat-driven ACS with different finned tube adsorber beds and working pairs.

Of the studies cited in Table 1, those with finned tube adsorber beds packed or coated with composite salts in porous matrixes, such as expanded graphite + NaBr [49] and $LiNO_3$-Silica KSK [38–40], and those packed with silicoaluminophosphate AQSOA FAM-Z02 [46] and Sapo-34 [54,55] had the highest SCP values. In a conceptual discussion on the optimal adsorbent for ACS applications, Aristov [12] highlighted the potential improvements in an ACS performance from using composite salts in porous matrixes, but leakage of salt solutions from the host matrixes during adsorption might cause corrosion of metal parts in an adsorber bed and, consequently, emission of non-condensable gases. Also, Okunev and Aristov [57] investigated the importance of adsorbent isobar shape on the SCP of an ACS. Their analysis indicated that with proper selection of an adsorbent material with respect to the operating conditions, the SCP could improve by a factor of 1.5 while other effective parameters, such as the adsorbent particle size, remained unchanged.

Ferroaluminophosphate (AQSOA FAM-Z01), silicoaluminophosphate (AQSOA FAM-Z02), and aluminophosphate (AQSOA FAM-Z05) are synthetic zeolite-based materials with high durability (60,000–200,000 cycles) developed for A/C and dehumidification applications by Mitsubishi Chemical Ltd [58]. These adsorbents have an "S" shaped adsorption isotherm, as shown in Refs. [59–61], which provides quick water adsorption and desorption within a narrow pressure range. Comparing the adsorption isotherms of FAM-Z01, FAM-Z02, and FAM-Z05 indicates that FAM-Z02 provides higher water vapor uptake capacity [59–62] and a broader desorption temperature (75–95 °C). For example, equilibrium water uptake differences of FAM-Z01 and FAM-Z02 at adsorption temperature of 30 °C and water vapor saturation temperature of 15 °C, and desorption temperature of 90 °C and water vapor saturation temperature of 30 °C are 0.185 and 0.254 $kg/kg_{dry\ adsorbent}$, respectively [63–66]. This shows that FAM-Z02 has 37% higher equilibrium water uptake than FAM-Z01 between adsorption and desorption. Therefore, in this study, FAM-Z02 adsorbent is used to pack the adsorber beds. Further details about FAM-Z02 properties including density, heat capacity, and equilibrium uptake rate have been reported in Refs. [60,61].

Sharafian et al. [67] experimentally showed the effects of different finned tube adsorber bed designs packed with 2 mm FAM-Z02 particles with respect to their heat transfer surface area and fin

Table 1
Performance analysis of different finned tube adsorber beds reported in the literature.

Ref. No.	Adsorber bed type and weight	Working pairs	Adsorbent packing method	COP	SCP (W/kg)	AAMR ($kg_{metal}/kg_{adsorbent}$)
[14–16]	Aluminum finned tube, 4.6 kg[a]	Activated carbon/ammonia	Consolidated	0.06[a]	33[a]	5.75[a]
[17]	SS[b] finned tube	Silica gel/methanol	Loose grain	–	30[a]	–
[18–20]	SS cylindrical double finned tube, 31 kg	Zeolite 13X/water	Loose grain	0.38	22.8[a]	5
[21,22]	176-finned tubes, 260 kg	Zeolite 13X/water	Loose grain	0.25	28.5	1.86
[23]	SS finned tube, 3.3 kg[a]	Silica gel + $CaCl_2$(SWS-1L)/water	Loose grain	0.43[a]	23.5[a]	3
[24]	2-bed Aluminum finned tube, 15 kg/bed	AQSOA FAM-Z02/water	Loose grain	0.27[a]	131.5[a]	7.9
[25–27]	2-bed finned tube, 32.7 kg/bed	Silica gel/water	Loose grain	0.43	48[a]	0.654
[28]	SS finned tube	Hydrophobic Y zeolite (CBV-901)/methanol	Coated	0.11[a]	25[a]	3
[29]	2-bed finned tube	Silica gel/water	Loose grain	0.29[a]	35[a]	–
[30–33]	2-bed finned tube	Act. carbon + $CaCl_2$ (1:4)/ammonia	Consolidated	0.19[a]	70.8[a]	–
[34]	Aluminum finned tube, 6.08 kg	Silica gel + $CaCl_2$(SWS-1L)/water	Coated	0.15	137[a]	3.47
[35]	Finned tube	Silica gel + $CaCl_2$/water	Loose grain	0.23	43	–
[36,37]	2-bed Aluminum finned tube, 13.6 kg/bed[a]	Silica gel/water	Loose grain	0.29	158[a]	4.53
[38–40]	Aluminum finned tube, 0.636 kg	$LiNO_3$-Silica KSK/water	Loose grain	0.18[a]	318[a]	1.82
[41,42]	28 finned tube with 2.5 mm fin spacing	Silica gel + LiCl/water	Loose grain	0.41	122	–
[43–45]	2-bed Aluminum finned tube	Silica gel + LiCl/methanol	Loose grain	0.41	76.5	–
		Silica gel/water	Loose grain	0.42	122	
[46]	2-bed Aluminum finned tube, 2.3 kg/bed	AQSOA FAM-Z02/water	Loose grain	0.45	330.2	1.4
[47,48]	8 tubes with Aluminum fins + steel pipes, 40 kg/bed	Expanded graphite + $CaCl_2$/ammonia	Loose grain	0.11	7.0	–
		Expanded graphite + $BaCl_2$/ammonia	Loose grain			
[49]	Carbon steel finned tube, 115 kg	Expanded graphite + NaBr/ammonia	Coated	0.35	296	20.9
[50]	4-bed SS shell and Aluminum finned tube	Silica gel/water	Loose grain	0.31	46.5[a]	–
[51]	2-bed finned tube	Expanded graphite + $CaCl_2$/ammonia	Loose grain	0.16	78.5	–
[52]	Aluminum finned tube, 0.16, 0.13, and 0.14 kg	AQSOA FAM-Z02/water	Loose grain	–	2300	1.78
						1.71
						1.92
[53]	3-bed Aluminum finned tube, 12.4 kg/bed	AQSOA FAM-Z02 + silica gel/water	Coated + Loose grain	–	296	1.85
[54,55]	Aluminum finned tube	Sapo-34/water	Coated	0.24	675	6
			Loose grain	0.4	498	1.96
[56]	2-bed copper finned tube	Zeolite 13X + $CaCl_2$/water	Loose grain	0.16	53	–

[a] These parameters are extracted based on the reported experimental data at $T_{hf,\ i} = 90$ °C, $T_{cf,\ i} = 30$ °C, $T_{coolant,\ i} = 30$ °C, and $T_{chilled,\ i} = 15$ °C. For zeolite 13X/water: $T_{hf,\ i} = 180$ °C.
[b] SS: Stainless steel.

spacing on in-situ water uptake rate measurements of FAM-Z02. The direct mass measurements showed that the adsorber bed with 2.8 m^2 heat transfer surface area and 2.5 mm fin spacing could increase the SCP and COP of the ACS by 3.1 and 2.9 times, respectively, in comparison with the adsorber bed with 0.235 m^2 heat transfer surface area and 8.5 mm fin spacing. Following these results, in this study, the adsorber bed with high heat transfer surface area and small fin spacing was installed in our ACS test bed to study the effects of the amount of adsorbent material and the number of adsorber beds on the SCP and COP of ACS when the other components of the cycle, namely, the condenser, evaporator and expansion valve, remained unchanged. Also, detailed parametric study was performed to investigate the effects of cycle time and operating conditions on the SCP and COP of ACS.

2. ACS thermodynamic cycle

The thermodynamic cycle of an ACS is comprised of two main steps: heating-desorption-condensation and cooling-adsorption-evaporation. An ACS with one adsorber bed generates evaporative cooling power intermittently. To produce a continuous cooling power, two or more adsorber beds are required, such as one shown in Refs. [68–70]. Fig. 1a depicts a schematic of a typical two-adsorber bed ACS comprised of two adsorber beds, a condenser, an expansion valve, and an evaporator.

Fig. 1b shows the thermodynamic processes in an ACS which is divided into two subcycles: (i) an adsorbent cycle (on the right side), and (ii) an adsorbate cycle (on the left side). As shown in Fig. 1b, the adsorbent cycle includes four steps: (1) isosteric heating (ih); process 1–2, (2) isobaric desorption (ibd); process 2–3′, (3) isosteric cooling (ic); process 3′-4′, and (4) isobaric adsorption (iba); process 4′-1. Isosteric processes occur at a constant specific volume and isobaric processes occur at a constant pressure. The adsorbate cycle shown in Fig. 1b includes three steps: (1) isobaric condensation in the condenser; process 2–3, (2) isenthalpic process in the expansion valve; process 3–4, and (3) isobaric evaporation in the evaporator; process 4–1.

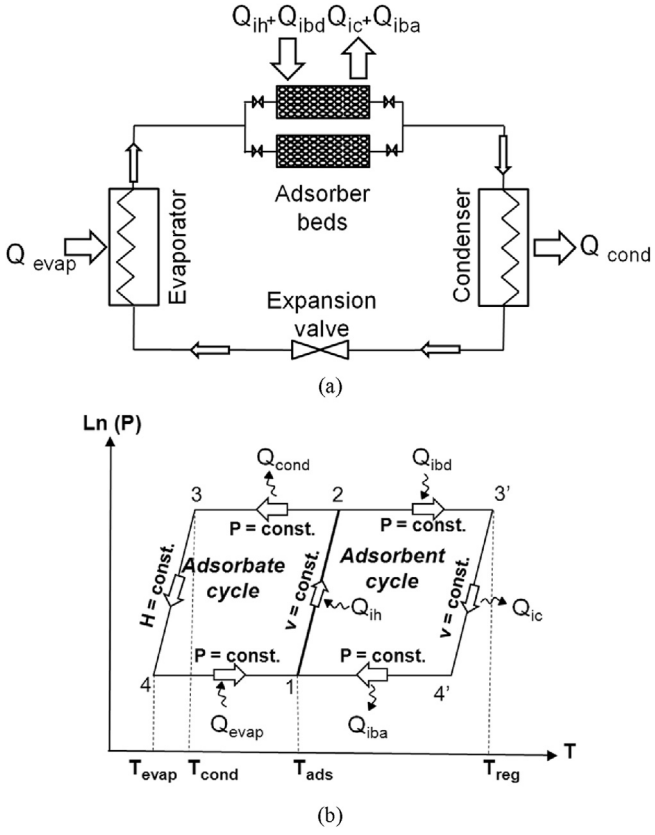

Fig. 1. (a) Schematic and (b) thermodynamic cycle of a two-adsorber bed ACS [71].

During step 1–2, the adsorbent-adsorbate pair absorbs heat of Q_{ih} from an external heat source in an isosteric heating process. In this step, the pressure of the adsorber bed increases due to the adsorbate desorption from the adsorbent particles. This process is continued until the pressure of the adsorber bed reaches the pressure of the condenser and then the inlet valve to the condenser is opened. In step 2–3′, the external heat source continuously heats the adsorber bed (Q_{ibd}) during an isobaric desorption process, the adsorbate leaves the adsorber bed, and is condensed inside the condenser through an isobaric condensation process (step 2–3). The total heat transfer to the adsorber bed, $Q_{total\ heating}$, during a desorption process is the sum of Q_{ih} and Q_{ibd}. Upon reaching point 3′, the maximum temperature of the adsorber bed at the end of desorption time, the valve between the adsorber bed and the condenser is closed and during an isosteric cooling process (step 3′-4′), the temperature of the adsorbent is reduced by dissipating the heat of Q_{ic} to a heat sink. In step 3–4, the adsorbate inside the condenser passes through the expansion valve and enters to the evaporator. During step 4–1, the adsorbate absorbs the heat of Q_{evap} from the environment of interest and evaporates. At the same time, the valve between the evaporator and the adsorber bed is opened and the adsorbent adsorbs the vaporous adsorbate through an isobaric adsorption process (step 4′-1) and releases heat of Q_{iba}. This process continues until reaching the end of adsorption time. The total heat removed from the adsorber bed, $Q_{total\ cooling}$, during an adsorption process is the sum of Q_{ic} and Q_{iba}. The cycle time is the sum of desorption and adsorption times.

3. Experimental test bed

An ACS with one or two adsorber beds made up of more than sixty different components was built in the lab. Fig. 2a shows a schematic of the two-adsorber bed ACS including heating and cooling circuits connected to the adsorber beds. The system was built modular to enable future modifications. The ACS was equipped with four temperature control systems (TCS) or thermal baths to control the adsorption and desorption temperatures in the adsorber beds, and the condensation and evaporation temperatures in the condenser and evaporator, respectively. Four check valves (V1–V4) with low cracking pressure were installed before and after the adsorber beds to control the adsorption and desorption processes, and eight two-way solenoid valves (V5–V12) were installed on the TCS_{HF} and TCS_{CF} to intermittently heat up and cool down adsorber beds 1 and 2 as shown in Fig. 2a. Further information about the valves and their arrangement can be found in Ref. [72].

Fig. 2b and c show the one- and two-adsorber bed ACS test beds including the main components. A copper shell-and-tube heat exchanger with helical fins on the outer surface of the tubes was used as the condenser. A needle valve with high precision flow adjustment was used as the expansion valve and a low-operating pressure evaporator with capillary-assisted tubes was designed and installed on the cycle. Type T thermocouples (Omega, model #5SRTC-TT-T-36-36) with accuracy of 0.75% of reading and pressure transducers with 0–34.5 kPa operating range (Omega, model #PX309-005AI) and 0.4 kPa accuracy were installed to monitor and record the temperature and pressure variations in each component of the ACS over time. Positive displacement flow meters (FLOMEC, Model # OM015S001-222) with accuracy of 0.5% of reading were installed on the adsorber beds to measure the heating and cooling

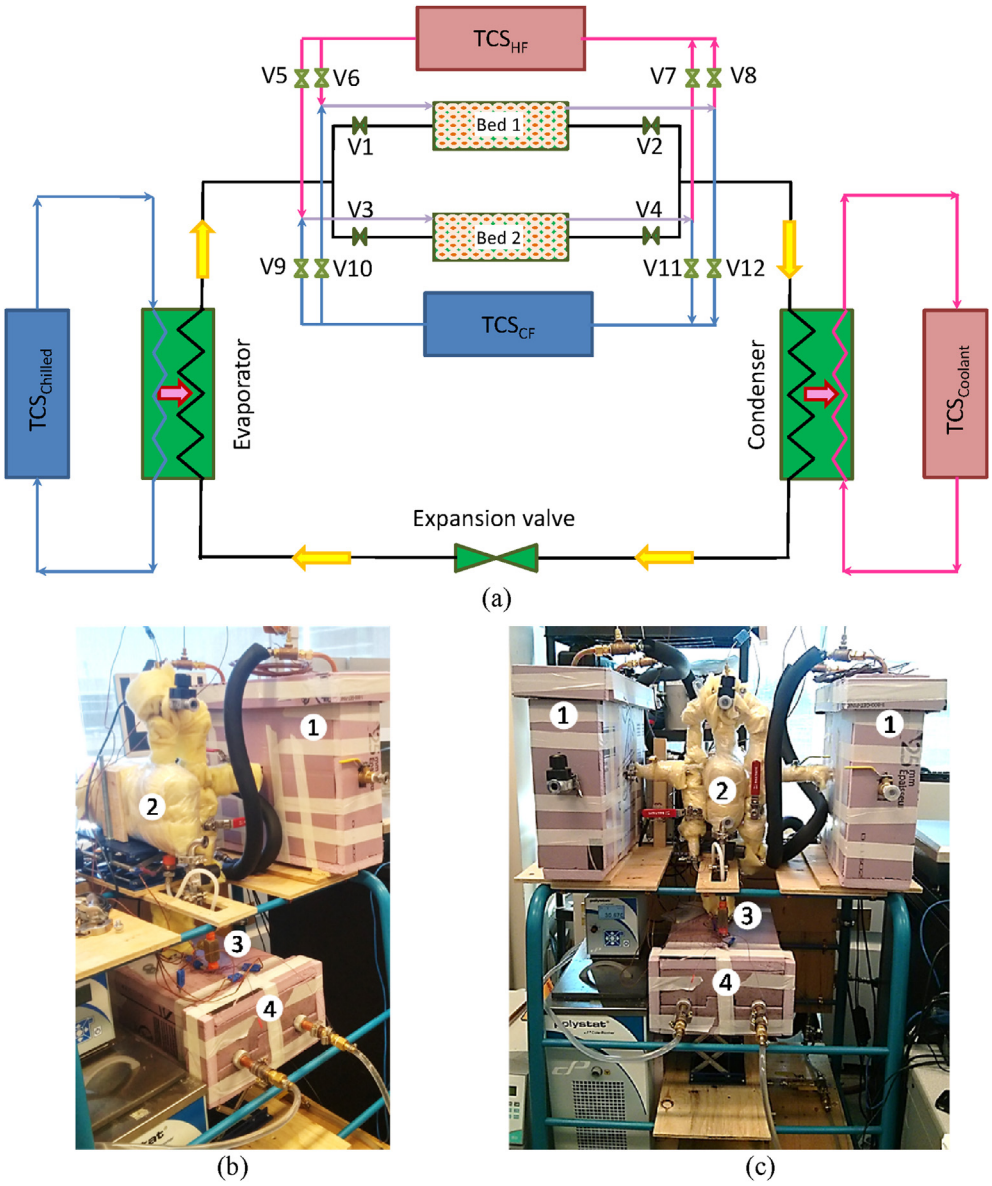

Fig. 2. (a) Schematic of the two-adsorber bed ACS (black line: adsorbate path, and blue and pink lines: heat transfer fluid paths), (b) the one- and (c) two-adsorber bed ACS experimental test beds. Numbers in (b) and (c): 1- adsorber bed(s), 2-condenser, 3-expansion valve, and 4-evaporator. (For interpretation of the references to colour in this figure legend, the reader is referred to the web version of this article.)

fluid flow rates. Similar flow meters were also installed on the condenser and evaporator to measure the coolant and chilled water flow rates, respectively. The heat transfer fluid used in the TCSs for heating and cooling of the adsorber beds was silicone oil (Julabo Inc., Thermal P60) that had a density change from 909 kg/m^3 at 30 °C to 854 kg/m^3 at 90 °C.

An engine oil cooler manufactured by Hayden Automotive (model #1268) was used as an adsorber bed, as shown in Fig. 3a, and was placed in custom-built vacuum chambers shown in Fig. 2b and c. Fig. 3b shows FAM-Z02 adsorbent particles packed in the adsorber bed. In this study, different amounts of adsorbent material (1.9, 1.0, and 0.5 kg) was packed in the adsorber bed to investigate their effects on the ACS performance. The intra-particle diffusion and inter-particle diffusion did not change for different amount of adsorbent because the thickness of adsorbent ("W" in Fig. 3a) was kept constant for all experiments. For 1.9 kg of adsorbent, the adsorber bed was packed fully. For 1.0 kg of adsorbent, the adsorber bed was packed in about half of the adsorber bed (H changed to ~ H/2 in Fig. 3a). Therefore, the heat transfer surface area reduced from 2.8 m^2 to 1.47 m^2. Similarly, for 0.5 kg of adsorbent, the adsorber bed was packed in about a quarter of the adsorber bed (H changed to H/2 and L changed to L/2 in Fig. 3a). This caused the heat transfer surface area to reduce to 0.74 m^2. Further details about the ACS test bed and operating conditions are summarized in Table 2.

Water was used in the ACS as the refrigerant (adsorbate) and, as a result, the ACS operated under vacuum pressure. To produce enough cooling inside the evaporator, the design of evaporator was different from the conventional evaporator designs [73]. A capillary-assisted evaporator was designed and installed on the system [74], as shown in Fig. 4. The tubes inside the evaporator had circumferential rectangular-cross sectional fins with 0.635 mm fin spacing (40 fins per inch (FPI)). Having small fin spacing assists water to fill the volume between two consecutive fins (groove) and cover the whole circumferential surface of the tube. Due to surface

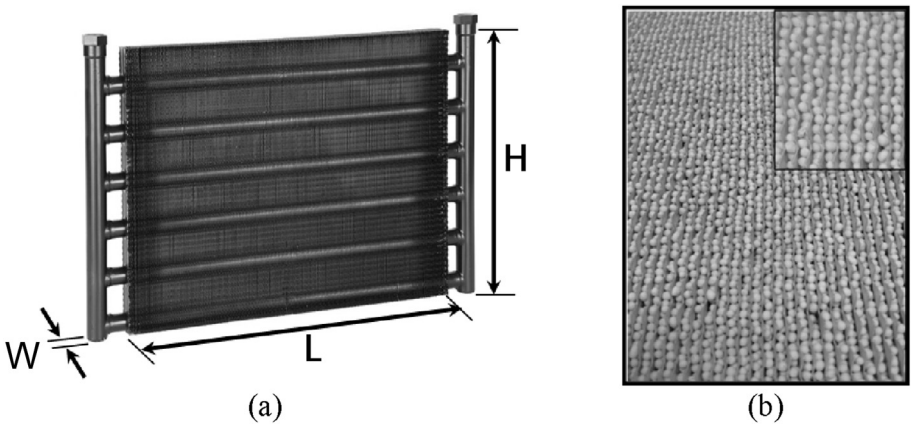

Fig. 3. (a) Heat exchanger used in the adsorber beds, and (b) FAM-Z02 adsorbent particles packed between fins of the adsorber bed.

Table 2
Specifications and operating conditions of the ACS built for this study.

Parameter	One-bed ACS	Two-bed ACS
Working pair	AQSOA FAM-Z02/water	
Adsorbent particles diameter (mm)	2	
Mass of adsorbent per adsorber bed (kg)	1.9/1.0/0.5	0.5
Adsorber bed heat transfer surface area, A_{bed}, (m^2)	2.80/1.47/0.74	0.74
Adsorber bed dimensions (L × W × H) (cm)	33.02 × 3.81 × 30.48 (13" × 1.5" × 12″)	
Adsorber bed fin spacing (mm)	2.54	
Metal mass of adsorber bed (kg)	2.87	
Heating fluid mass flow rate to adsorber bed (kg/s)	0.058 (4.1 L/min of silicone oil)	
Cooling fluid mass flow rate to adsorber bed (kg/s)	0.062 (4.1 L/min of silicone oil)	
Heat capacity of heating and cooling fluids (kJ/kg.K)	1.8	
Condenser heat transfer surface area, A_{cond}, (m^2)	2.0	
Coolant water mass flow rate to condenser (kg/s)	0.052 (3.1 L/min)	
Evaporator heat transfer surface area, A_{evap}, (m^2)	0.405	
Chilled water mass flow rate to evaporator (kg/s)	0.037 (2.2 L/min)	
Heating fluid inlet temperature to adsorber bed (°C)	90	
Cooling fluid inlet temperature to adsorber bed (°C)	30	
Coolant water inlet temperature to condenser (°C)	30	
Chilled water inlet temperature to evaporator (°C)	15	
Cycle time (min)	20	

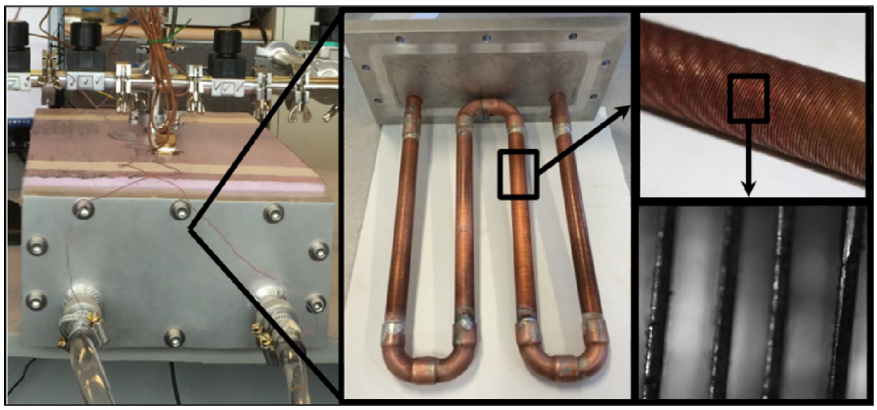

Fig. 4. Capillary-assisted evaporator designed by Thimmaiah et al. [74].

tension, the liquid-vapor interface inside the rectangular-groove forms a curvature which increases gradually along the circumferential direction [75]. The extended meniscus region is comprised of a non-evaporating region, evaporating thin film region, and bulk region [76]. Heat transfer is concentrated at the evaporating thin film region where the liquid film is extremely thin and the thermal resistance is very low. This creates an effective evaporating flow [77]. Further geometric details of the capillary-assisted evaporator are provided in Table 3.

Before running the experiments, the adsorber beds packed with the FAM-Z02 were heated using a 90 °C heating fluid for 8 h and simultaneously evacuated to completely dry the FAM-Z02 out. The heating and cooling fluid inlet temperatures to the adsorber beds, and the coolant and chilled water inlet temperatures to the

Table 3
Geometric details of the capillary-assisted evaporator [74].

Parameter	Value
Tube model	Turbo Chil-40 FPI (Wolverine Tube Inc.)
Outer diameter (mm)	19.05 (3/4″)
Fin type	Continuous and parallel fins
Number of fins per meter	1575 (40 fins per inch)
Fin spacing (mm)	0.635
Fin Height (mm)	1.473
Min. wall under fins (mm)	0.635
Inside surface area (m^2/m)	0.051
Outside surface area (m^2/m)	0.263
Tube length (m)	1.54

condenser and evaporator were set at temperatures given in Table 2. By setting the cycle time, water was adsorbed and desorbed by FAM-Z02 particles packed in the adsorber beds, and condensation and evaporation occurred inside the condenser and evaporator, respectively. An experiment at constant operating conditions was performed continuously until the dynamic behavior of the ACS became consistent. At this stage, the thermodynamic cycle of ACS was repeated three more times to ensure the reproducibility of the collected data.

4. Data analysis

To evaluate the performance of an ACS, the COP and SCP of the system should be calculated. Eq. (1) gives the total evaporative cooling energy during an adsorption process:

$$Q_{evap}(J) = \int_{adsorption} \dot{m}_{chilled} c_{p,chilled} \left(T_{chilled,i} - T_{chilled,o}\right) dt \quad (1)$$

where $\dot{m}_{chilled}$ and $c_{p,chilled}$ are the chilled water mass flow rate and heat capacity, and $T_{chilled,i} - T_{chilled,o}$ is the temperature difference between the chilled water inlet and outlet temperatures. The total condensation energy is calculated as follows:

$$Q_{cond}(J) = \int_{desorption} \dot{m}_{coolant} c_{p,coolant} \left(T_{coolant,i} - T_{coolant,o}\right) dt \quad (2)$$

where $\dot{m}_{coolant}$ is the coolant water mass flow rate and $T_{coolant,i} - T_{coolant,o}$ is the temperature difference between the coolant water inlet and outlet temperatures. The total heat transfers to the adsorber beds during an adsorption or desorption process are calculated by:

$$Q_{total\ \ cooling}(J) = \int_{adsorption} \dot{m}_{cf} c_{p,cf} \left(T_{cf,i} - T_{cf,o}\right) dt \quad (3)$$

$$Q_{total\ \ heating}(J) = \int_{desorption} \dot{m}_{hf} c_{p,hf} \left(T_{hf,i} - T_{hf,o}\right) dt \quad (4)$$

where $\dot{m}_{cf}$ and $\dot{m}_{hf}$ are the cooling and heating fluid mass flow rates, and $T_{cf,i} - T_{cf,o}$ and $T_{hf,i} - T_{hf,o}$ are the temperature differences between the cooling and heating fluid inlet and outlet temperatures, respectively. Using Eqs. (1) and (4), the COP and SCP of an ACS during one cycle are determined by:

$$COP = \frac{Q_{evap}}{Q_{total\ \ heating}} \quad (5)$$

$$SCP(W/kg) = \frac{Q_{evap}}{m_{adsorbent}\tau_{cycle}} \quad (6)$$

where $m_{adsorbent}$ in Eq. (6) is the mass of dry adsorbent packed inside an adsorber bed and τ_{cycle} is the cycle time (sum of adsorption and desorption times). The maximum uncertainties in the calculations of COP and SCP were 13% and 11%, respectively (see the Appendix).

5. Results and discussion

5.1. Effects of adsorbent mass on the performance of a one-adsorber bed ACS

The one-adsorber bed ACS was packed with three different amounts of FAM-Z02 (1.9, 1.0, and 0.5 kg). The adsorber bed packed with more adsorbent mass creates higher suction and discharge pressures during adsorption and desorption, respectively. However, the evaporator and condenser should be able to supply sufficient evaporation and condensation rates, respectively. In the case of a mismatch between these components, the overall performance of ACS is affected.

Fig. 5 shows the temperature and pressure variations inside the one-adsorber bed ACS packed with 1.0 kg of FAM-Z02 at cycle time of 20 min. It can be seen that the dynamic behavior of ACS is consistent for three continuous cycles and, as a result, the performance of the system is reproducible. During adsorption, uptake of the vapor by the adsorbent material lowers the adsorber bed pressure, P_{bed}, to less than the evaporator pressure, $P_{evap.}$ During this process, marked “Ads.” in Fig. 5, the adsorber bed temperature is maintained by the cooling fluid that dissipates the heat of adsorption. Due to the suction pressure created by the adsorber bed, evaporation happens inside the evaporator, heat is transferred from the chilled water to the adsorbate, and the chilled water temperature reduces at the outlet of the evaporator, $T_{chilled,\ o}$, as shown in Fig. 5a. In a desorption process, the adsorber bed is heated, as shown in the region demarcated “Des.” in Fig. 5, and the adsorber bed pressure, P_{bed}, increases, as shown in Fig. 5b. Due to the pressure gradient between the adsorber bed and the condenser, the adsorbate desorbed from the FAM-Z02 flows to the condenser. Condensation happens inside the condenser and heat of condensation is transferred from the adsorbate to the coolant water. Therefore, the coolant water outlet temperature, $T_{coolant,\ o}$, increases as shown in Fig. 5a.

The 206–260 Pa pressure difference between the adsorber bed and the evaporator during adsorption shown in Fig. 5b indicates that the adsorbate evaporation rate in the evaporator is not sufficient to supply enough water vapor to the FAM-Z02 packed in the adsorber bed. The mismatch between the water uptake rate of FAM-Z02 and the water evaporation rate inside the evaporator significantly affect the SCP and COP of the system. Fig. 6 shows the effects of different adsorber bed loads of FAM-Z02 (0.5, 1.0, 1.9 kg) on the SCP and COP of the one-adsorber bed ACS under different cycle times. It can be seen in Fig. 6 that lowering the amount of FAM-Z02 increases the SCP of the system, while it lowers the COP. Increasing the SCP of the ACS by decreasing the mass of the FAM-Z02 from 1.9 to 0.5 kg under a constant cycle time indicates the enough vaporous adsorbate supply to the FAM-Z02 during adsorption. However, the COP of ACS decreases by decreasing the mass of FAM-Z02 under a constant cycle time because the AAMR increases from 1.5 to 5.7 kg $_{metal}$/kg $_{dry\ adsorbent}$.

Lambert and Jones [78] reported that the total daily commute time in the U.S. was about 40 min, ≈20 min to work and ≈20 min returning home. Therefore, the cycle time of 20 min was selected

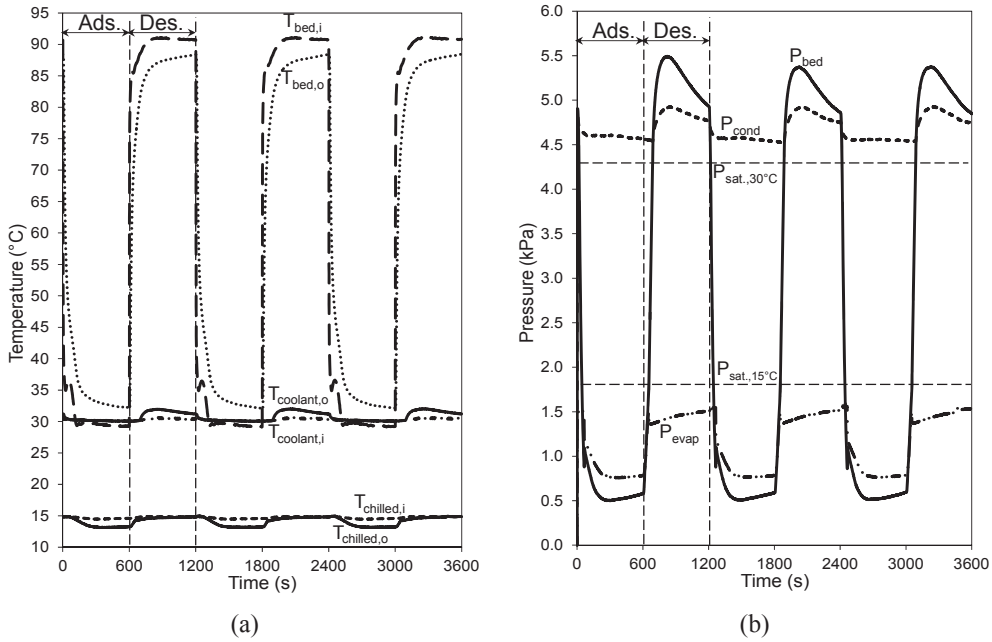

Fig. 5. Temperature and pressure variations in different components of the ACS for 1.0 kg of FAM-Z02 and cycle time of 20 min (other operating conditions are as given in Table 2).

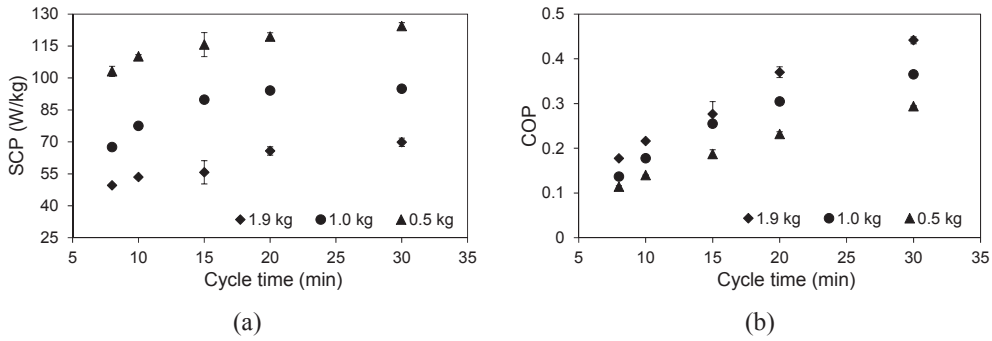

Fig. 6. Variations in SCP and COP of the one-adsorber bed ACS packed with different amounts of FAM-Z02 vs. cycle time (Other operating conditions are as given in Table 2).

for further analysis of the performance of the one-adsorber bed ACS. Effects of heating and cooling fluid inlet temperatures to the adsorbed bed on the SCP and COP of ACS are shown in Fig. 7. It can be seen in Fig. 7a and b that by increasing the heating fluid inlet temperature from 70 to 90 °C, the SCP and COP of the system increase. As shown in Fig. 7a, at a heating fluid inlet temperature of 70 °C, the adsorber bed with 1.9 kg of FAM-Z02 provides the SCP of 38.7 W/kg which is 45% higher than that with 0.5 kg of FAM-Z02. At the heating inlet temperatures of 80 and 90 °C, however, the SCPs of ACS with 0.5 kg of FAM-Z02 are 78.8 and 119 W/kg which are 15% and 82% higher than those packed with 1.9 kg of FAM-Z02, respectively. Such a behavior is not observed in the COP of the ACS, as shown in Fig. 7b. At a constant heating fluid inlet temperature, the COP decreases by decreasing the mass of FAM-Z02 from 1.9 to 0.5 kg because of the increase in the AAMR.

Increasing the cooling fluid inlet temperature to the adsorber bed reduces the SCP and COP of the ACS for all three masses of FAM-Z02 as shown in Fig. 7c and d. The results also show that at a specific cooling fluid inlet temperature, increasing the mass of FAM-Z02 decreases the SCP and increases the COP of ACS. Finally, Fig. 7 indicates that the performance of ACS packed with FAM-Z02 is more sensitive to the heating fluid inlet temperature (desorption temperature) rather than the cooling fluid inlet temperature (adsorption temperature).

Increasing the coolant water inlet temperature to the condenser decreases the rate of adsorbate condensation inside the condenser and therefore reduces the SCP and COP of the system as shown in Fig. 8a and b. The FAM-Z02 is only partially dried out under these cycle conditions. Increasing the mass of FAM-Z02 at a constant coolant water inlet temperature causes the SCP to decrease and the COP to increase.

Increasing the chilled water inlet temperature to the evaporator increases the water evaporation rate and the evaporator pressure, and consequently, more adsorbate is supplied to the FAM-Z02 within a constant adsorption time. As shown in Fig. 8c and d, increasing the chilled water inlet temperature increases the SCP and COP of ACS. Further, the SCP of the ACS increases and the COP decreases when the mass of FAM-Z02 reduces from 1.9 to 0.5 kg. As discussed in Section 1, the SCP of an ACS designed for vehicle A/C applications is more important than the COP as the waste heat available from an ICE is abundant. As a result, the adsorber bed packed with 0.5 kg of FAM-Z02 is considered for the next set of experiments.

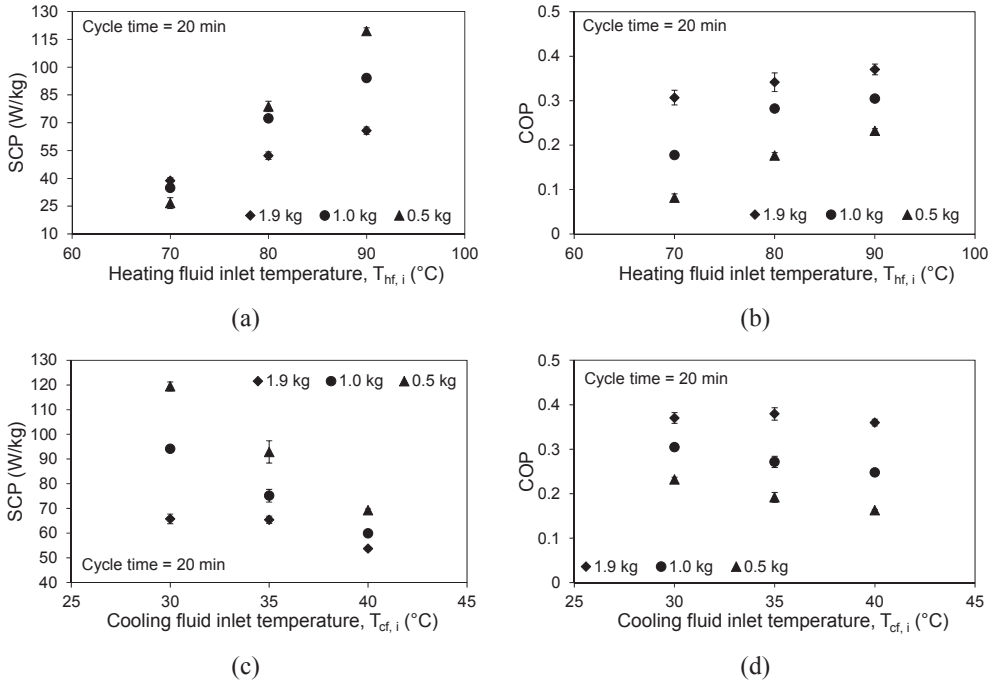

Fig. 7. Variations in SCP and COP of the one-adsorber bed ACS packed with different amounts of FAM-Z02 vs. heating and cooling fluid inlet temperatures entering to the adsorber bed (Other operating conditions are as given in Table 2).

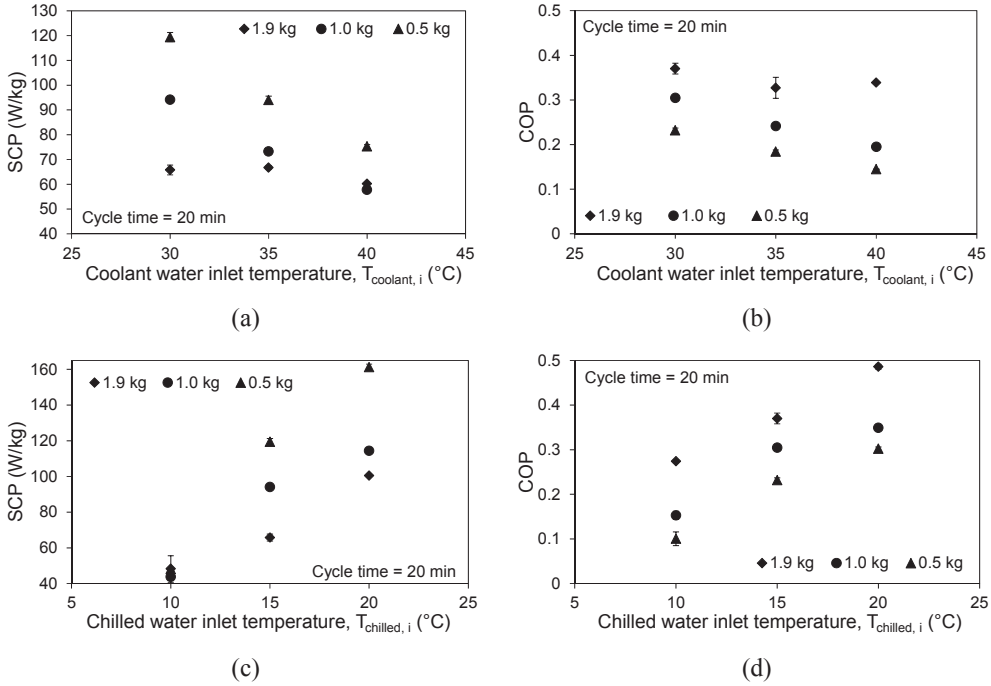

Fig. 8. Variations in SCP and COP of the one-adsorber bed ACS packed with different amounts of FAM-Z02 vs. coolant and chilled water inlet temperatures entering to the condenser and evaporator (Other operating conditions are as given in Table 2).

5.2. Effects of the number of adsorber beds on the performance of an ACS

One of the limitations of the one-adsorber bed ACS was intermittent cooling power generation in the evaporator, especially for short cycle times, when the thermal mass of the evaporator became important. The thermal mass of the evaporator in an ACS postpones the heat transfer from the chilled water to the adsorbate inside the evaporator. Multi-adsorber bed systems produce continuous cooling in the evaporator. However, increasing the number of adsorber beds adds to the overall mass and complexity of the ACS. Knowing these limitations, a second adsorber bed was added to the one-adsorber bed ACS and its performance was studied and compared against that of the one-adsorber bed ACS.

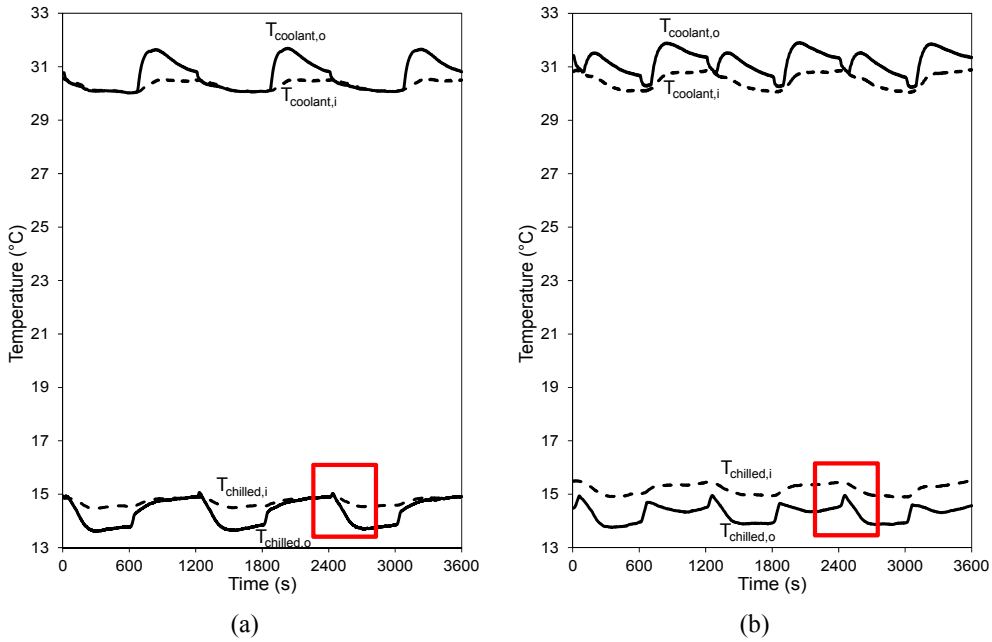

Fig. 9. Coolant and chilled water inlet and outlet temperature variations in (a) the one-adsorber bed ACS and (b) the two-adsorber bed ACS packed with 0.5 kg of FAM-Z02 and cycle time of 20 min (Other operating conditions are as given in Table 2).

The coolant and chilled water temperature variations in the one- and two-adsorber bed ACS packed with 0.5 kg of FAM-Z02 and cycle time of 20 min are shown in Fig. 9. The regions demarcated on the chilled water temperatures in Fig. 9 indicate that the chilled water outlet temperature in the two-adsorber bed ACS is more uniform than that in the one-adsorber bed ACS and does not reach to the chilled water inlet temperature because of continuous evaporation inside the evaporator. Therefore, the effect of thermal mass of the evaporator becomes less important to the performance of ACS especially for short cycle times.

The effects of one- and two-adsorber bed ACS on the SCP under different cycle times are shown in Fig. 10a. The SCP of one-adsorber bed ACS increases continuously as the cycle time increases from 8 to 30 min. However, the SCP of two-adsorber bed ACS peaks at 152.5 W/kg for a cycle time of 20 min before decreasing to 132.0 W/kg for a cycle time of 30 min. Fig. 10a indicates that the two-adsorber bed ACS resulted in higher SCPs under short cycle times (8–20 min). By increasing the cycle time from 20 to 30 min, the effect of thermal mass of evaporator becomes less important and the SCP of two-adsorber bed ACS drops.

The COP of the two-adsorber bed ACS is higher than that of one-adsorber bed ACS as shown in Fig. 10b. At a cycle time of 8 min, the COPs of one- and two-adsorber bed ACS are 0.11 and 0.12, respectively. At a cycle time of 20 min, the COP of two-adsorber bed ACS in comparison with that of one-adsorber bed ACS increases by 47% from 0.23 to 0.34. The highest COP, 0.39, is observed for the two-adsorber bed ACS operated with the 30 min cycle time. However, considering both the SCP and COP, the two-adsorber bed ACS has the best performance at cycle time of 20 min.

Fig. 11 shows the effects of heating and cooling fluid inlet temperatures to the adsorber beds on the performance of the one- and two-adsorber bed ACS packed with 0.5 kg of FAM-Z02 and operated with a 20 min cycle time. Fig. 11 shows that, at constant heating and cooling fluid inlet temperatures, the SCP and COP increase by replacing the one-adsorber bed ACS with the two-adsorber bed ACS. At heating fluid inlet temperature of 70 °C, shown in Fig. 11a and b, the SCP and COP of two-adsorber bed ACS are equal to 52.6 W/kg and 0.17 which are 98% and 105% higher than those of the one-adsorber bed ACS. Similarly, Fig. 11c and d show that at the cooling fluid inlet temperature of 40 °C, the SCP and COP of two-adsorber bed ACS are 51% and 47% higher than those of one-adsorber bed ACS.

The effects of coolant and chilled water inlet temperatures to the condenser and evaporator on the SCP and COP of one- and two-adsorber bed ACS are shown in Fig. 12. It can be seen in Fig. 12a and b that increasing the coolant water inlet temperature from 30

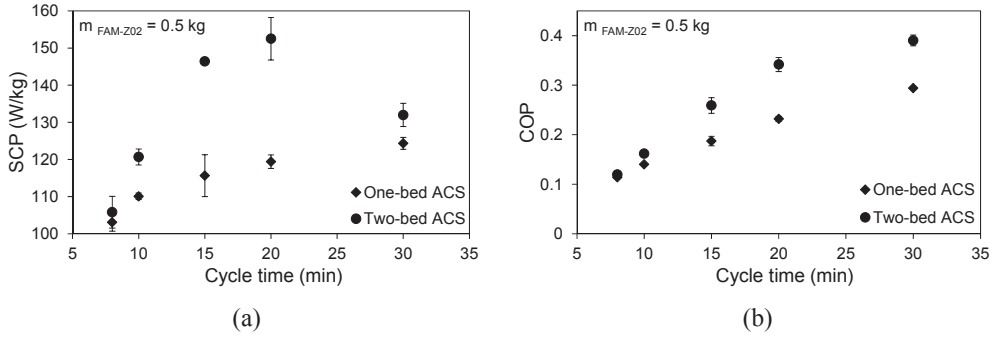

Fig. 10. Variations in SCP and COP of the one- and two-adsorber bed ACS packed with 0.5 kg of FAM-Z02 vs. cycle time (Other operating conditions are as given in Table 2).

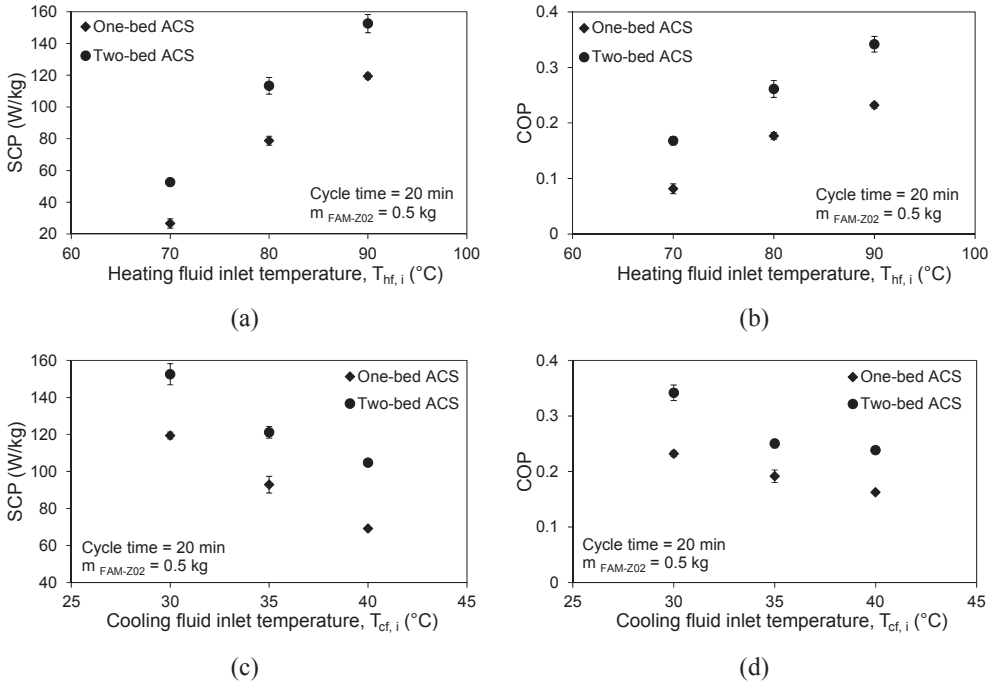

Fig. 11. Variations in SCP and COP of the one- and two-adsorber bed ACS packed with 0.5 kg of FAM-Z02 vs. (a, b) heating and (c, d) cooling fluid inlet temperatures entering to the adsorber beds (Other operating conditions are as given in Table 2).

to 40 °C, decreases the SCP and COP of ACS because of the reduce in the adsorbate condensation rate during desorption. Also, Fig. 12a and b display that the SCP and COP of two-adsorber bed ACS is always higher than those of one-adsorber bed ACS under different coolant water inlet temperatures to the condenser.

Fig. 12c and d show that the SCP and COP of ACS increase with increasing the chilled water inlet temperature to the evaporator. The SCP and COP of two-adsorber bed ACS increase from 78 W/kg and 0.17 at 10 °C to 191.5 W/kg and 0.35 at 20 °C. Similar to previous cases, the SCP and COP of the two-adsorber bed ACS are always higher than those of one-adsorber bed ACS.

6. Conclusion

In this study, the effects of adsorbent mass and the number of adsorber beds on the SCP and COP of ACS were investigated. A

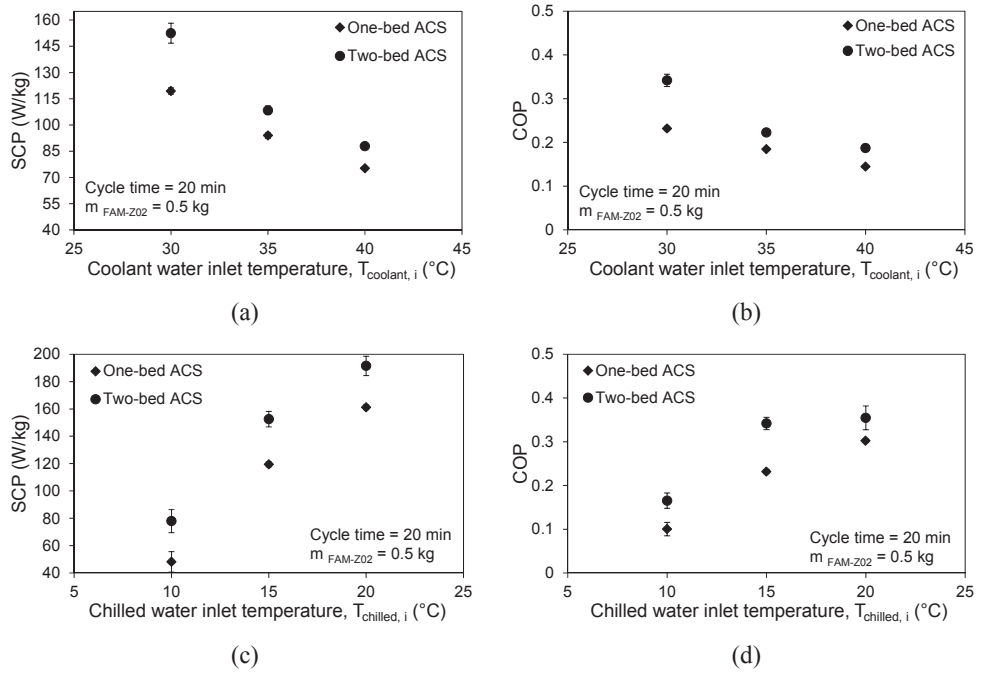

Fig. 12. Variations in SCP and COP of the one- and two-adsorber bed ACS packed with 0.5 kg of FAM-Z02 vs. (a, b) coolant and (c, d) chilled water inlet temperatures entering to the condenser and evaporator (Other operating conditions are as given in Table 2).

comprehensive parametric study was performed to investigate the variations of SCP and COP of ACS under different cycle times and operating conditions. Three different amounts of FAM-Z02 were packed in the one-adsorber bed ACS. The results showed that reducing the mass of FAM-Z02 from 1.9 to 0.5 kg increased the SCP of the ACS while the COP decreased due to the increase in the AAMR. Also, the results showed that the thermal mass of the evaporator reduced the SCP and COP of ACS under short cycle times (8–20 min). Addition of the second adsorber bed to the one-adsorber bed ACS indicated that the SCP and COP increased by 28% and 47% at cycle time of 20 min. Also, the results showed that the SCP and COP of the two-adsorber bed ACS were always higher than those of the one-adsorber bed ACS due to the reduction in the effects of the thermal mass of the evaporator especially at short cycle times. Finally, from this study, it could be concluded that the mass of adsorbent packed in adsorber beds should be optimized to reach the highest performance of the ACS and reduce the overall of mass of the system.

Acknowledgment

The authors gratefully acknowledge the financial support of the Natural Sciences and Engineering Research Council of Canada (NSERC) through the Automotive Partnership Canada Grant No. APCPJ 401826-10.

Appendix

The systematic uncertainty in the evaporative cooling energy calculations, Eq. (1), is:

$$\left(\frac{\delta Q_{evap}}{Q_{evap}}\right)_{systematic} = \sqrt{\left(\frac{\delta \dot{m}_{chilled}}{\dot{m}_{chilled}}\right)^2 + \left(\frac{\delta\left(T_{chilled,i} - T_{chilled,o}\right)}{T_{chilled,i} - T_{chilled,o}}\right)^2} \tag{7}$$

where,

$$\frac{\delta\left(T_{chilled,i} - T_{chilled,o}\right)}{T_{chilled,i} - T_{chilled,o}} = \sqrt{\left(\frac{\delta T_{chilled,i}}{T_{chilled,i}}\right)^2 + \left(\frac{\delta T_{chilled,o}}{T_{chilled,o}}\right)^2} = \sqrt{0.0075^2 + 0.0075^2} = 0.01 \tag{8}$$

Therefore, the maximum systematic uncertainty in the calculation of evaporative cooling energy is:

$$\left(\frac{\delta Q_{evap}}{Q_{evap}}\right)_{systematic} \times 100 = \sqrt{0.005^2 + 0.01^2} \times 100 = 1\% \tag{9}$$

Also, the maximum standard deviation for Q_{evap} due to the random uncertainties in the experiments was 10%. As a result, the maximum uncertainty in the calculation of Q_{evap} during the experiments was 11% (1% + 10%). Similarly, the maximum uncertainty in the calculation of $Q_{total\ \ heating}$ was 7% (= 1% + 6%). Therefore, the maximum uncertainties in the calculations of COP and SCP were as follows:

$$\frac{\delta COP}{COP} \times 100 = \sqrt{\left(\frac{\delta Q_{evap}}{Q_{evap}}\right)^2 + \left(\frac{\delta Q_{total\ heating}}{Q_{total\ heating}}\right)^2} \times 100 = \sqrt{0.11^2 + 0.07^2} \times 100 = 13\% \tag{10}$$

$$\frac{\delta SCP}{SCP} \times 100 = \sqrt{\left(\frac{\delta Q_{evap}}{Q_{evap}}\right)^2 + \left(\frac{\delta m_{adsorbent}}{m_{adsorbent}}\right)^2 + \left(\frac{\delta \tau_{cycle}}{\tau_{cycle}}\right)^2} \times 100 = \sqrt{0.11^2 + \left(\frac{1}{500}\right)^2 + \left(\frac{1}{1800}\right)^2} \times 100 = 11\% \tag{11}$$

Nomenclature

A	heat transfer surface area (m^2)
$AAMR$	adsorber bed to adsorbent mass ratio ($kg_{\ metal}/kg_{\ dry\ adsorbent}$)
$Ads.$	adsorption
c_p	heat capacity at constant pressure ($J/kg.K$)
COP	coefficient of performance
$Des.$	desorption
m	mass (kg)
$\dot{m}$	mass flow rate (kg/s)
P	pressure (kPa)
Q	heat transfer (J)
SCP	specific cooling power ($W/kg_{\ dry\ adsorbent}$)
T	temperature (K)
t	time (s)
τ_{cycle}	cycle time (s)

Subscripts

adsorbate	adsorbate
adsorbent	adsorbent particles
bed	adsorber bed
cf	cooling fluid
chilled	chilled water
cond	condenser
coolant	coolant water
evap	evaporator
hf	heating fluid
i	in
o	out
sat.	saturation

References

[1] Buzelin LOS, Amico SC, Vargas JVC, Parise JAR. Experimental development of an intelligent refrigeration system. Int J Refrig 2005;28:165–75. http://dx.doi.org/10.1016/j.ijrefrig.2004.08.013.
[2] Farrington R, Rugh J. Impact of vehicle air-conditioning on fuel economy, tailpipe emissions, and electric vehicle range. In: Proceeding earth technol. Forum, Washington, D.C; 2000.
[3] Suzuki M. Application of adsorption cooling systems to automobiles. Heat Recover Syst CHP 1993;13:335–40.
[4] Abdullah MO, Tan IAW, Lim LS. Automobile adsorption air-conditioning system using oil palm biomass-based activated carbon: a review. Renew Sustain Energy Rev 2011;15:2061–72. http://dx.doi.org/10.1016/j.rser.2011.01.012.
[5] Demir H, Mobedi M, Ülkü S. A review on adsorption heat pump: problems and solutions. Renew Sustain Energy Rev 2008;12:2381–403. http://dx.doi.org/10.1016/j.rser.2007.06.005.
[6] Poyelle F, Guilleminot JJ, Meunier F. Experimental tests and predictive model of an adsorptive air conditioning unit. Ind Eng Chem Res 1999;38:298–309. http://dx.doi.org/10.1021/ie9802008.
[7] Tamainot-Telto Z, Critoph RE. Monolithic carbon for sorption refrigeration and heat pump applications. Appl Therm Eng 2001;21:37–52. http://dx.doi.org/10.1016/S1359-4311(00)00030-2.
[8] Freni A, Tokarev MM, Restuccia G, Okunev AG, Aristov YI. Thermal conductivity of selective water sorbents under the working conditions of a sorption chiller. Appl Therm Eng 2002;22:1631–42. http://dx.doi.org/10.1016/S1359-4311(02)00076-5.
[9] Sharafian A, Fayazmanesh K, McCague C, Bahrami M. Thermal conductivity and contact resistance of mesoporous silica gel adsorbents bound with

polyvinylpyrrolidone in contact with a metallic substrate for adsorption cooling system applications. Int J Heat Mass Transf 2014;79:64–71. http://dx.doi.org/10.1016/j.ijheatmasstransfer.2014.07.086.
[10] Sharafian A, Bahrami M. Adsorbate uptake and mass diffusivity of working pairs in adsorption cooling systems. Int J Heat Mass Transf 2013;59:262–71. http://dx.doi.org/10.1016/j.ijheatmasstransfer.2012.12.019.
[11] Askalany AA, Salem M, Ismael IM, Ali AHH, Morsy MG, Saha BB. An overview on adsorption pairs for cooling. Renew Sustain Energy Rev 2013;19:565–72. http://dx.doi.org/10.1016/j.rser.2012.11.037.
[12] Aristov Y. Concept of adsorbent optimal for adsorptive cooling/heating. Appl Therm Eng 2014;72:166–75. http://dx.doi.org/10.1016/j.applthermaleng.2014.04.077.
[13] Sharafian A, Bahrami M. Assessment of adsorber bed designs in waste-heat driven adsorption cooling systems for vehicle air conditioning and refrigeration. Renew Sustain Energy Rev 2014;30:440–51. http://dx.doi.org/10.1016/j.rser.2013.10.031.
[14] Critoph RE. Towards a one tonne per day solar ice maker. Renew Energy 1996;9:626–31. http://dx.doi.org/10.1016/0960-1481(96)88366-2.
[15] Tamainot-Telto Z, Critoph RE. Adsorption refrigerator using monolithic carbon-ammonia pair. Int J Refrig 1997;20:146–55.
[16] Critoph RE. Rapid cycling solar/biomass powered adsorption refrigeration system. Renew Energy 1999;16:673–8.
[17] Oertel K, Fischer M. Adsorption cooling system for cold storage using methanol/silicagel. Appl Therm Eng 1998;18:773–86. http://dx.doi.org/10.1016/S1359-4311(97)00107-5.
[18] Zhang LZ, Wang L. Momentum and heat transfer in the adsorbent of a waste-heat adsorption cooling system. Energy 1999;24:605–24. http://dx.doi.org/10.1016/S0360-5442(99)00018-3.
[19] Zhang LZ, Wang L. Effects of coupled heat and mass transfers in adsorbent on the performance of a waste heat adsorption cooling unit. Appl Therm Eng 1999;19:195–215.
[20] Zhang LZ. Design and testing of an automobile waste heat adsorption cooling system. Appl Therm Eng 2000;20:103–14. http://dx.doi.org/10.1016/S1359-4311(99)00009-5.
[21] Jiangzhou S, Wang RZ, Lu YZ, Xu YX, Wu JY. Experimental investigations on adsorption air-conditioner used in internal-combustion locomotive driver-cabin. Appl Therm Eng 2002;22:1153–62. http://dx.doi.org/10.1016/S1359-4311(02)00036-4.
[22] Lu YZ, Wang RZ, Jianzhou S, Zhang M, Xu Y, Wu J. Performance of a diesel locomotive waste-heat-powered adsorption air conditioning system. Adsorption 2004;10:57–68.
[23] Restuccia G, Freni A, Vasta S, Aristov YI. Selective water sorbent for solid sorption chiller: experimental results and modelling. Int J Refrig 2004;27:284–93. http://dx.doi.org/10.1016/j.ijrefrig.2003.09.003.
[24] Magnetto D. Thermally operated mobile air conditioning systems. 2005.
[25] Wang DC, Xia ZZ, Wu JY, Wang RZ, Zhai H, Dou WD. Study of a novel silica gel–water adsorption chiller. Part I. Design and performance prediction. Int J Refrig 2005;28:1073–83. http://dx.doi.org/10.1016/j.ijrefrig.2005.03.001.
[26] Wang DC, Wu JY, Xia ZZ, Zhai H, Wang RZ, Dou WD. Study of a novel silica gel–water adsorption chiller. Part II. Experimental study. Int J Refrig 2005;28:1084–91. http://dx.doi.org/10.1016/j.ijrefrig.2005.03.002.
[27] Wang DC, Shi ZX, Yang QR, Tian XL, Zhang JC, Wu JY. Experimental research on novel adsorption chiller driven by low grade heat source. Energy Convers Manag 2007;48:2375–81. http://dx.doi.org/10.1016/j.enconman.2007.03.001.
[28] Restuccia G, Freni A, Russo F, Vasta S. Experimental investigation of a solid adsorption chiller based on a heat exchanger coated with hydrophobic zeolite. Appl Therm Eng 2005;25:1419–28. http://dx.doi.org/10.1016/j.applthermaleng.2004.09.012.
[29] Yang GZ, Xia ZZ, Wang RZ, Keletigui D, Wang DC, Dong ZH, et al. Research on a compact adsorption room air conditioner. Energy Convers Manag 2006;47:2167–77. http://dx.doi.org/10.1016/j.enconman.2005.12.005.
[30] Wang LW, Wang RZ, Lu ZS, Chen CJ, Wu JY. Comparison of the adsorption performance of compound adsorbent in a refrigeration cycle with and without mass recovery. Chem Eng Sci 2006;61:3761–70. http://dx.doi.org/10.1016/j.ces.2006.01.018.
[31] Lu ZS, Wang RZ, Wang LW, Chen CJ. Performance analysis of an adsorption refrigerator using activated carbon in a compound adsorbent. Carbon N. Y 2006;44:747–52. http://dx.doi.org/10.1016/j.carbon.2005.09.016.
[32] Wang LW, Wang RZ, Lu ZS, Chen CJ, Wang K, Wu JY. The performance of two adsorption ice making test units using activated carbon and a carbon composite as adsorbents. Carbon N. Y 2006;44:2671–80. http://dx.doi.org/10.1016/j.carbon.2006.04.013.
[33] Chen CJ, Wang RZ, Wang LW, Lu ZS. Studies on cycle characteristics and application of split heat pipe adsorption ice maker. Energy Convers Manag 2007;48:1106–12. http://dx.doi.org/10.1016/j.enconman.2006.10.017.
[34] Freni A, Russo F, Vasta S, Tokarev M, Aristov YI, Restuccia G. An advanced solid sorption chiller using SWS-1L. Appl Therm Eng 2007;27:2200–4. http://dx.doi.org/10.1016/j.applthermaleng.2005.07.023.
[35] Daou K, Wang RZ, Xia ZZ, Yang GZ. Experimental comparison of the sorption and refrigerating performances of a CaCl2 impregnated composite adsorbent and those of the host silica gel. Int J Refrig 2007;30:68–75. http://dx.doi.org/10.1016/j.ijrefrig.2006.05.003.
[36] Verde M, Corberan JM, de Boer R, Smeding S. Modelling of a waste heat driven silica gel/water adsorption cooling system comparison with experimental results. Int Sorpt Heat Pump Padua, Italy 2011:7–8.
[37] Sapienza A, Santamaria S, Frazzica A, Freni A. Influence of the management strategy and operating conditions on the performance of an adsorption chiller. Energy 2011;36:5532–8. http://dx.doi.org/10.1016/j.energy.2011.07.020.
[38] Aristov YI, Sapienza A, Ovoshchnikov DS, Freni A, Restuccia G. Reallocation of adsorption and desorption times for optimisation of cooling cycles. Int J Refrig 2012;35:525–31. http://dx.doi.org/10.1016/j.ijrefrig.2010.07.019.
[39] Sapienza A, Glaznev IS, Santamaria S, Freni A, Aristov YI. Adsorption chilling driven by low temperature heat: new adsorbent and cycle optimization. Appl Therm Eng 2012;32:141–6. http://dx.doi.org/10.1016/j.applthermaleng.2011.09.014.
[40] Freni A, Sapienza A, Glaznev IS, Aristov YI, Restuccia G. Experimental testing of a lab-scale adsorption chiller using a novel selective water sorbent "silica modified by calcium nitrate." Int J Refrig 2012;35:518–24. http://dx.doi.org/10.1016/j.ijrefrig.2010.05.015.
[41] Gong LX, Wang RZ, Xia ZZ, Chen CJ. Design and performance prediction of a new generation adsorption chiller using composite adsorbent. Energy Convers Manag 2011;52:2345–50. http://dx.doi.org/10.1016/j.enconman.2010.12.036.
[42] Lu ZS, Wang RZ. Study of the new composite adsorbent of salt LiCl/silica gel–methanol used in an innovative adsorption cooling machine driven by low temperature heat source. Renew Energy 2014;63:445–51. http://dx.doi.org/10.1016/j.renene.2013.10.010.
[43] Lu ZS, Wang RZ, Xia ZZ, Wu QB, Sun YM, Chen ZY. An analysis of the performance of a novel solar silica gel–water adsorption air conditioning. Appl Therm Eng 2011;31:3636–42. http://dx.doi.org/10.1016/j.applthermaleng.2010.11.024.
[44] Lu Z, Wang R, Xia Z, Gong L. Experimental investigation adsorption chillers using micro-porous silica gel–water and compound adsorbent-methanol. Energy Convers Manag 2013;65:430–7. http://dx.doi.org/10.1016/j.enconman.2012.09.018.
[45] Lu ZS, Wang RZ. Performance improvement and comparison of mass recovery in CaCl 2/activated carbon adsorption refrigerator and silica gel/LiCl adsorption chiller driven by low grade waste heat. Int J Refrig 2013;36:1504–11. http://dx.doi.org/10.1016/j.ijrefrig.2013.03.008.
[46] Vasta S, Freni A, Sapienza A, Costa F, Restuccia G. Development and lab-test of a mobile adsorption air-conditioner. Int J Refrig 2012;35:701–8. http://dx.doi.org/10.1016/j.ijrefrig.2011.03.013.
[47] Wang J, Wang LW, Luo WL, Wang RZ. Experimental study of a two-stage adsorption freezing machine driven by low temperature heat source. Int J Refrig 2013;36:1029–36. http://dx.doi.org/10.1016/j.ijrefrig.2012.10.029.
[48] Song FP, Gong LX, Wang LW, Wang RZ. Study on gradient thermal driven adsorption cycle with freezing and cooling output for food storage. Appl Therm Eng 2014;70:231–9. http://dx.doi.org/10.1016/j.applthermaleng.2014.04.066.
[49] Kiplagat JK, Wang RZ, Oliveira RG, Li TX, Liang M. Experimental study on the effects of the operation conditions on the performance of a chemisorption air conditioner powered by low grade heat. Appl Energy 2013;103:571–80. http://dx.doi.org/10.1016/j.apenergy.2012.10.025.
[50] San J-Y, Tsai F-K. Testing of a lab-scale four-bed adsorption heat pump. Appl Therm Eng 2014;70:274–81. http://dx.doi.org/10.1016/j.applthermaleng.2014.05.014.
[51] Pan QW, Wang RZ, Lu ZS, Wang LW. Experimental investigation of an adsorption refrigeration prototype with the working pair of composite adsorbent-ammonia. Appl Therm Eng 2014;72. http://dx.doi.org/10.1016/j.applthermaleng.2014.06.054.
[52] Santamaria S, Sapienza A, Frazzica A, Freni A, Girnik IS, Aristov YI. Water adsorption dynamics on representative pieces of real adsorbers for adsorptive chillers. Appl Energy 2014;134:11–9. http://dx.doi.org/10.1016/j.apenergy.2014.07.053.
[53] Freni A, Bonaccorsi L, Calabrese L, Caprì A, Frazzica A, Sapienza A. SAPO-34 coated adsorbent heat exchanger for adsorption chillers. Appl Therm Eng 2015;82:1–7. http://dx.doi.org/10.1016/j.applthermaleng.2015.02.052.
[54] Frazzica A, Sapienza A, Freni A. Novel experimental methodology for the characterization of thermodynamic performance of advanced working pairs for adsorptive heat transformers. Appl Therm Eng 2013;72:229–36. http://dx.doi.org/10.1016/j.applthermaleng.2014.07.005.
[55] Gullì G, Sapienza A, Caprì A, Costa F, La Rosa D, Palomba V, et al. Innovative adsorption chiller for marine applications: design and building. Energy Proced 2015;82:432–8. http://dx.doi.org/10.1016/j.egypro.2015.11.831.
[56] Tso CY, Chan KC, Chao CYH, Wu CL. Experimental performance analysis on an adsorption cooling system using zeolite 13X/CaCl2 adsorbent with various operation sequences. Int J Heat Mass Transf 2015;85:343–55. http://dx.doi.org/10.1016/j.ijheatmasstransfer.2015.02.005.
[57] Okunev BN, Aristov YI. Making adsorptive chillers faster by a proper choice of adsorption isobar shape: comparison of optimal and real adsorbents. Energy 2014;76:400–5. http://dx.doi.org/10.1016/j.energy.2014.08.031.
[58] Himooka SS, Shima KO. The evaluation of direct cooling and heating desiccant device coated with FAM. J Chem Eng Jpn 2007;40:1330–4.
[59] Henninger SK, Schmidt FP, Henning HM. Water adsorption characteristics of novel materials for heat transformation applications. Appl Therm Eng 2010;30:1692–702. http://dx.doi.org/10.1016/j.applthermaleng.2010.03.028.
[60] Okamoto K, Teduka M, Nakano T, Kubokawa S, Kakiuchi H. The development of AQSOA water vapor adsorbent and AQSOA coated heat exchanger. In: Int. Symp. Innov. Mater. Process. Energy syst., Singapor; 2010.
[61] Goldsworthy MJ. Measurements of water vapour sorption isotherms for RD

silica gel, AQSOA-Z01, AQSOA-Z02, AQSOA-Z05 and CECA zeolite 3A. Microporous Mesoporous Mater 2014;196:59–67. http://dx.doi.org/10.1016/j.micromeso.2014.04.046.
[62] Dawoud B. On the effect of grain size on the kinetics of water vapor adsorption and desorption into/from loose pellets of FAM-Z02 under a typical operating condition of adsorption heat pumps. J Chem Eng Jpn 2007;40:1298–306. http://dx.doi.org/10.1252/jcej.07WE163.
[63] Kim YD, Thu K, Ng KC. Adsorption characteristics of water vapor on ferroaluminophosphate for desalination cycle. Desalination 2014;344:350–6. http://dx.doi.org/10.1016/j.desal.2014.04.009.
[64] Myat A, Kim Choon N, Thu K, Kim YD. Experimental investigation on the optimal performance of Zeolite-water adsorption chiller. Appl Energy 2013;102:582–90. http://dx.doi.org/10.1016/j.apenergy.2012.08.005.
[65] Newalkar BL, Jasra RV, Kamath V, Bhat SGT. Sorption of water in aluminophosphate molecular sieve AlPO4-5. Microporous Mesoporous Mater 1998;20:129–37. http://dx.doi.org/10.1016/S1387-1811(97)00021-8.
[66] Thu K, Kim YD, Xi BJ, Ismail A, Ng KC. Thermophysical properties of novel zeolite materials for sorption cycles. Appl Mech Mater 2013;388:116–22. doi:10.4028/www.scientific.net/AMM.388.116.
[67] Sharafian A, Nemati Mehr SM, Huttema W, Bahrami M. Effects of different adsorber bed designs on in-situ water uptake rate measurements of AQSOA FAM-Z02 for vehicle air conditioning applications. Appl Therm Eng 2016;98:568–74.
[68] Saha BB, Koyama S, Lee JB, Kuwahara K, Alam KC, Hamamoto Y, et al. Performance evaluation of a low-temperature waste heat driven multi-bed adsorption chiller. Int J Multiph Flow 2003;29:1249–63. http://dx.doi.org/10.1016/S0301-9322(03)00103-4.
[69] Jribi S, Saha BB, Koyama S, Chakraborty A, Ng KC. Study on activated carbon/HFO-1234ze(E) based adsorption cooling cycle. Appl Therm Eng 2013;50:1570–5. http://dx.doi.org/10.1016/j.applthermaleng.2011.11.066.
[70] Jribi S, Saha BB, Koyama S, Bentaher H. Modeling and simulation of an activated carbon–CO2 four bed based adsorption cooling system. Energy Convers Manag 2014;78:985–91. http://dx.doi.org/10.1016/j.enconman.2013.06.061.
[71] Sharafian A, Bahrami M. A quasi steady state model for adsorption cooling systems: automotive applications. In: ASME 2012 6th int. Conf. Energy sustain. 10th fuel cell sci. Eng. Technol. Conf., San Diego, CA, USA; 2012.
[72] Sharafian A, Dan PC, Huttema W, Bahrami M. Performance analysis of a novel expansion valve and control valves designed for a waste heat-driven two-adsorber bed adsorption cooling system. Appl Therm Eng 2016;100:1119–29.
[73] Wang RZ, Wang L, Wu J. Adsorption refrigeration technology: theory and application. John Wiley & Sons; 2014.
[74] Cheppudira Thimmaiah P, Sharafian A, Huttema W, Bahrami M. Effects of capillary-assisted tubes with different fin geometries on the performance of a low-operating pressure evaporator for adsorption cooling systems. Appl Energy 2016;171:256–65.
[75] Nilson RH, Tchikanda SW, Griffiths SK, Martinez MJ. Steady evaporating flow in rectangular microchannels. Int J Heat Mass Transf 2006;49:1603–18. http://dx.doi.org/10.1016/j.ijheatmasstransfer.2005.11.002.
[76] Ma HB, Cheng P, Borgmeyer B, Wang YX. Fluid flow and heat transfer in the evaporating thin film region. Microfluid Nanofluidics 2008;4:237–43. http://dx.doi.org/10.1007/s10404-007-0172-5.
[77] Ma HB, Peterson GP. Temperature variation and heat transfer in triangular grooves with an evaporating film. J Thermophys Heat Transf 1997;11:90–7. http://dx.doi.org/10.2514/2.6205.
[78] Lambert MA, Jones BJ. Automotive adsorption air conditioner powered by exhaust heat. Part 1: conceptual and embodiment design. Proc Inst Mech Eng Part D J Automob Eng 2006;220:959–72. http://dx.doi.org/10.1243/09544070JAUTO221.